RSC Advances

PAPER

View Article Online
View Journal | View Issue

Cite this: *RSC Adv.*, 2020, **10**, 21309

Dielectric control of porous polydimethylsiloxane elastomers with Au nanoparticles for enhancing the output performance of triboelectric nanogenerators†

Merreta Noorenza Biutty,[a] Ja Min Koo,[a] Maulida Zakia,[a] Puji Lestari Handayani,[a] U Hyeok Choi[b] and Seong Il Yoo*[a]

Received 20th April 2020
Accepted 29th May 2020

DOI: 10.1039/d0ra03522j

rsc.li/rsc-advances

Taking advantage of the triboelectrification effect and electrostatic induction, triboelectric nanogenerators (TENGs) provide a simple and efficient path to convert environmental mechanical energy into electric energy. Since the generation of surface charges and their density on triboelectric materials are the key factors in determining TENG performance, many efforts have been undertaken to engineer the structures and chemistry of triboelectric materials. Among others, dielectric control of triboelectric materials is an emerging approach because the dielectric constant is intimately correlated with the capacitance of materials. In this regard, we prepared porous polydimethylsiloxane (PDMS) composites decorated with Au nanoparticles (NPs), which was designed to engineer the compressibility and dielectric constant of PDMS elastomer. To this end, a polydopamine layer was synthesized on the PDMS surface to facilitate the homogeneous deposition of Au NPs. Unlike untreated PDMS sponges, Au NPs were efficiently coated onto polydopamine-treated PDMS sponges to increase the dielectric constant. When the resulting porous NP-PDMS composites were assembled into TENG devices, the electrical output of the TENGs initially improved but decreased with the amount of Au NPs. This trade-off relationship has been discussed in terms of charge generation on the air surface and pores of NP-PDMS composites based on a recent experimental model.

Introduction

The extraction of electric energy from environmental and biological sources has attracted a great deal of attention in recent years in order to supply power for micro-electronics as well as solve the global energy crisis.[1–7] Among many energy-harvesting techniques, triboelectric nanogenerators (TENGs) represent a simple and efficient approach that is based on triboelectrification and electrostatic induction.[3,4,8–15] In TENGs, surface charge transfer occurs by mechanical contact between two materials with different triboelectric polarities.[3,4,16] When separated, the two oppositely charged materials induce an electric potential difference, which in turn drives the electron flow through an external load.[3,4,8–15] Since the electric potential difference in TENGs is regulated by the distance between the two charged surfaces, electricity can be generated in response to the successive contact and separation of component structures by mechanical vibration.[3,4,8–15] Understanding that the generation of surface charges and their density on the triboelectric materials are the key factors in determining the output performance of TENGs, many research groups have engineered interfacial structures and/or surface chemistry to optimize the charge transfer process.[8–15] For instance, the formation of micro-patterns such as pyramid, cube, and lines,[8,9] utilization of electro-spun nanofibers,[10,11] and introduction of inorganic structures[12,13] have been employed to increase the contact area. In addition, surface modification with self-assembled monolayers (SAMs)[14] or polymers[15] has engineered the triboelectric sequence of the given materials for better control of the triboelectric properties.

Recently, it has been further demonstrated that the charge density on triboelectric materials is closely correlated with their capacitance.[17–25] Since capacitance, which is the capability to hold charges at a given potential, is proportional to the ratio of the dielectric constant (ε) to the thickness of triboelectric materials (d), the ratio of ε/d has been adjusted to optimize the electric output from TENGs.[17–25] For instance, polydimethylsiloxane (PDMS) elastomers have been blended with inorganic nanoparticles (NPs),[17,18] or new polymers such as poly(*tert*-butyl acrylate)-grafted polyvinylidene difluoride

[a]*Department of Polymer Engineering, Pukyong National University, Busan 48547, Korea. E-mail: siyoo@pknu.ac.kr; Tel: +82-51-629-6456*

[b]*Department of Polymer Science and Engineering, Inha University, Incheon 22212, Korea*

† Electronic supplementary information (ESI) available. See DOI: 10.1039/d0ra03522j

copolymers[19] have been synthesized to increase the dielectric constant. With the increased dielectric property, the surface charges on the triboelectric materials increased substantially, which resulted in improved power generation.[17–19] Comparable approach for the dielectric control has been also investigated in piezoelectric nanogenerators to enhance their output performance. In particular, inorganic fillers such as carbon nanotubes, graphene oxide, metal nanoparticles have been introduced in poly(vinylidene fluoride) (PVDF) matrix to increase the dielectric property of the PVDF composites and also to induce piezoelectric crystal phases.[26–28]

Alternatively, nano- or micro-scale pores have been introduced into PDMS elastomers to reduce the thickness of PDMS under external pressure.[20,21] Because of the fact that the charge transfer occurs under mechanical contact between two materials, namely, PDMS and metal, the compressed PDMS can accommodate more surface charges due to the increased capacitance, in comparison with a flat film-based PDMS. From this perspective, one can further anticipate that the ε/d value could be better engineered by introducing inorganic NPs with a high dielectric constant and pores simultaneously in the triboelectric materials. Recently, Baik *et al.* prepared Au NP-embedded mesoporous PDMS by a simple evaporation method, in which Au NPs were placed at the bottom side of the pores by gravitational force.[22] Alternatively, PDMS elastomers were blended with inorganic NPs and NaCl (or sugar) powder, from which pores were created by removing NaCl (or sugar) by the H_2O rinsing step.[23,24] These porous NP-PDMS composites are interesting because they can provide increased capacitance and additional charge can be generated from each pore by mechanical contact between the NPs and the inner surface of the pores.

Understanding that charge generation from individual pores in the porous NP-PDMS composites is an important factor for enhancing the TENG performance, it is necessary to decorate the surface of PDMS pores by inorganic NPs. However, the direct attachment of inorganic NPs to the surface of PDMS pores is strongly limited by the chemical inertness of PDMS. Although plasma treatment has been previously utilized for the surface modification of PDMS for the NP attachment,[29,30] this method cannot be applicable for the porous structures. In this study, in order to address this issue, we utilized a polydopamine (PDA) layer as an adhesive interface for PDMS and Au NPs. Dopamine is a small molecule consisting of catechol and amine and can be spontaneously polymerized into a thin film onto numerous types of surfaces.[31–33] Since PDA coating is based on the diffusion and *in situ* polymerization of dopamine monomers, PDA coating would be suitable for the surface modification of porous materials.[31,32] In addition, the coated PDA thin film has intrinsic metal binding ability owing to the catechol moiety.[31–33] This can facilitate the deposition of Au NPs onto PDA-coated PDMS. It also needs to be noted that the utilization of PDA for the uniform coating of NPs on the inner surface of PDMS pores has not been reported in TENG devise. Based on this perspective, we present a simple and versatile method for the preparation of NP-decorated PDMS sponges with the aid of a PDA polymer. In particular, we demonstrate that the amount of NPs deposited on the PDMS sponges could be engineered by simply adjusting the immersion time of PDA-coated PDMS sponges into an aqueous solution of Au NPs. We found that the open-circuit voltage and short-circuit current initially increased with the amount of Au NPs, but decreased under higher NP content. This trade-off relationship has been discussed in terms of charge generation on the air surface and pores of the NP-PDMS composites.

Experimental

Polydimethylsiloxane (PDMS) SYLGARD 184 Silicone Elastomer base and thermal curing agent were obtained from Dow Chemical Company. Dopamine hydrochloride (98%), trizma base (>99.9%), gold(III) chloride trihydrate (99.9%), and sodium citrate tribasic dihydrate (99.0%) were purchased from Sigma-Aldrich. All chemicals were used as received.

Porous PDMS sponges were prepared according to literature with a minor modification.[34] Commercial sugar powder was kneaded by adding deionized water and then cast onto a mold (3 cm × 2 cm × 1 cm) to prepare the sugar template. After being dried and peeled off from the mold, two prepared sugar templates were placed onto a Petri dish, at which a mixture (3 g) of PDMS prepolymer and curing agent was present at a weight ratio of 10 : 1. Subsequently, the Petri dish was placed in vacuum at room temperature for 4 h to degas the PDMS mixture. In this step, the PDMS mixture was infiltrated into the pores of the sugar templates by capillary force. After curing the PDMS at 80 °C for 2 h, the sugar template was dissolved in deionized water, which resulted in the PDMS sponges having three-dimensionally interconnected pores. In parallel, Au NPs (12 nm diameter) were synthesized by a citrate reduction method.[35] Briefly, an aqueous solution of sodium citrate tribasic dihydrate (0.5 g in 25 mL) was injected into a boiling aqueous solution of $HAuCl_4$ (0.1 g in 500 mL) and the mixture was stirred for 15 min and then cooled to room temperature. The resulting solution was centrifuged at 9000 rpm for 40 min to remove excess citrate, and the precipitated Au NPs were re-dispersed in deionized water. The absorbance of Au NPs in an aqueous solution was adjusted to 1.0 in all cases.

To decorate the surface of PDMS pores with Au NPs, polydopamine (PDA) polymers were introduced as an adhesive layer. For this purpose, a growth solution was prepared by dissolving dopamine monomer (2 mg mL^{-1}) in 10 mM Tris buffer (pH = 8.5). Then, the prepared PDMS sponge was immersed in the growth solution for 4 h to synthesize PDA polymers on the surface of PDMS. After the polymerization of the PDA layer, the PDMS sponges were washed by immersion in deionized water overnight. Finally, the PDA-coated PDMS sponge was further immersed in an aqueous solution (20 mL) of Au NPs for different periods of time (0–60 h). The prepared PDMS/PDA/Au sponge was washed using deionized water and dried for 2 days under ambient conditions.

The TENG was prepared by assembling the prepared PDMS/PDA/Au sponge (3 cm × 2 cm × 0.5 cm), two acrylic substrates (5 cm × 5 cm × 0.5 cm), and copper electrodes. First, four corners of acrylic substrates were drilled to create holes for

spring installation. Then, two pieces of copper foil (4 cm × 2 cm) were glued onto the acrylic substrates by Kapton film as electrodes onto which a conducting wire was additionally connected for electric measurement. As a triboelectric layer, a PDMS/PDA/Au sponge was attached to the bottom electrode. Finally, four springs were installed into the drilled holes to assemble the acrylic substrates together, leaving an air gap of ~3 mm between the copper electrode and the triboelectric layer.

UV-Vis absorbance data were obtained using a UV-Visible spectrophotometer (Agilent Cary 8454). Particle size distribution and zeta potential were evaluated by dynamic light scattering (DLS) using a Malvern Zetasizer Nano ZS90. Field-emission scanning electron microscopy (FE-SEM) images were taken using a Hitachi High-Technologies S-4800 instrument. Transmission electron microscopy (TEM) was performed using a Hitachi H-7500 instrument operating at 80 kV. Sample for TEM were prepared by drying a drop of Au NP solution onto a carbon-coated copper grid at room temperature. Attenuated total reflectance Fourier transform infrared (ATR-FTIR) spectra were obtained using a JASCO FT/IR-4100 spectrometer. To measure the output performance of the TENG, a periodic compressive force was repeatedly applied to the top surface of the TENG in such a way that the thickness of the PDMS/PDA/Au sponge was compressed from 5 mm to 3 mm. The short circuit current and open-circuit voltage of the TENG were measured using a Keithley 6514. The dielectric measurements of PDMS, PDMS/PDA, and PDMS/PDA/Au were performed by impedance spectroscopy using a Bio-Logic VSP-300 potentiostat, with a 10 mV amplitude and a 10^3 to 10^7 Hz frequency range.

Results and discussion

To enhance the capacitance of triboelectric materials, we attempted to simultaneously introduce porous structures and inorganic nanoparticles to triboelectric materials to increase the value of the ε/d ratio. For this purpose, we first prepared porous PDMS elastomers using the sugar-template method. Although several techniques have been proposed for the preparation of porous PDMS elastomers,[17,20–24,34] the sugar-template method represents a simple, cost-effective, and shape/size-tunable approach.[20,34] In this method, the sugar template is first prepared by pouring the kneaded sugars into a pre-made mold. By infiltrating PDMS prepolymers into the pores of the sugar template, porous PDMS elastomers can be replicated by curing the PDMS prepolymers, followed by rinsing the sugar template with water. As shown in Fig. 1a, the replicated PDMS sponge can be repeatedly compressed and recovered without mechanical deterioration. In addition, the white appearance of PDMS, which would be caused by light scattering from the internal surface of the PDMS elastomer, may indicate the

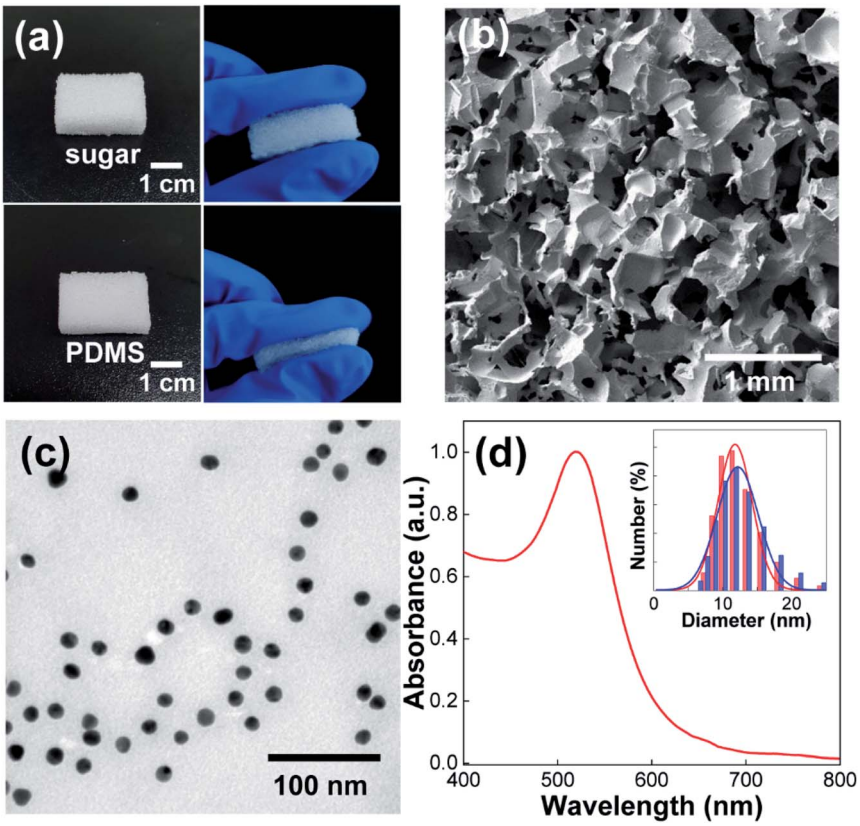

Fig. 1 (a) Photographs of the sugar template and replicated PDMS elastomer. (b) Plan-view SEM image of the porous PDMS sponge. (c and d) TEM image (c) and UV-Vis spectrum (d) of the synthesized Au NPs. The DLS results with Gaussian fittings before (red color) and after (blue color) centrifugation-based purification are shown in Fig. 1d.

presence of porous structures. When the micro-structures of the PDMS replica were examined by FE-SEM (Fig. 1b), the presence of pores (300–500 μm) can be clearly discernible from the three-dimensionally interconnected PDMS frame. It should be noted that the SEM image in Fig. 1b was collected from the air surface of the PDMS sponge; however, mainly identical structure was observed from the cross-sectional area of the PDMS replica.

Confirming the formation of the porous PDMS elastomer, we synthesized Au NPs using the citrate-reduction method as an inorganic counterpart.[35] Although other inorganic NPs could be utilized, Au NPs were selected as model NPs because of their chemical stability, easy synthesis, and structural uniformity. As shown in the TEM image (Fig. 1c), the synthesized Au NPs were uniform in size and shape. Since the Au NPs could be aggregated during centrifugation-based purification process, we compared the size distribution of Au NPs before and after the centrifugation. In the DLS result (inset of Fig. 1d), the size distribution of Au NPs was remained the same after the centrifugation, ruling out the possible NP aggregation. From the Gaussian fitting of the DLS result, the average diameter of Au NPs was determined to be 12 nm. In addition, Au NPs exhibited a well-known localized surface plasmon resonance (LSPR) peak at 520 nm (Fig. 1d),[36] which further confirmed NP synthesis. In the UV-Vis spectra, the absorbance peak of Au NPs at 520 nm was adjusted as 1.0. Since the molar extinction coefficient of 12 nm Au NPs is 1.89×10^8 M^{-1} cm^{-1},[37] the NP concentration was calculated as 5.3 nM by Lambert–Beer law. It needs to be noted that the synthesized Au NPs have negative charges on the surface (zeta potential = −33.2 mV) owing to the citrate molecules. This strongly restricts the adsorption of NPs onto the hydrophobic surface of the PDMS sponges. In this regard, we introduced polydopamine (PDA) layer as an adhesive interface for PDMS and Au NPs from the following experiment.

To synthesize the PDA polymer, PDMS sponges (Fig. 1b) were immersed in a dopamine solution in Tris buffer (pH = 8.5) for 4 h. Note that dopamine monomers spontaneously undergo oxidative polymerization in alkaline conditions to form a PDA coating on virtually all types of surfaces.[31,32] In particular, it has been reported that PDA can be coated on the PDMS surface to reduce the hydrophobicity of PDMS as well as to promote chemical and/or physical interactions with other molecules by the catechol and amine groups in PDA molecules.[38–40] Therefore, it can be anticipated that the PDA layer behaves as an adhesive interface for binding Au NPs and PDMS surfaces. After the polymerization, the white color of the PDMS sponge turned brown, which strongly indicated the synthesis of PDA on the PDMS surface. The same brown color also appeared when the cross-sectioned PDMS surface was examined. Therefore, it is

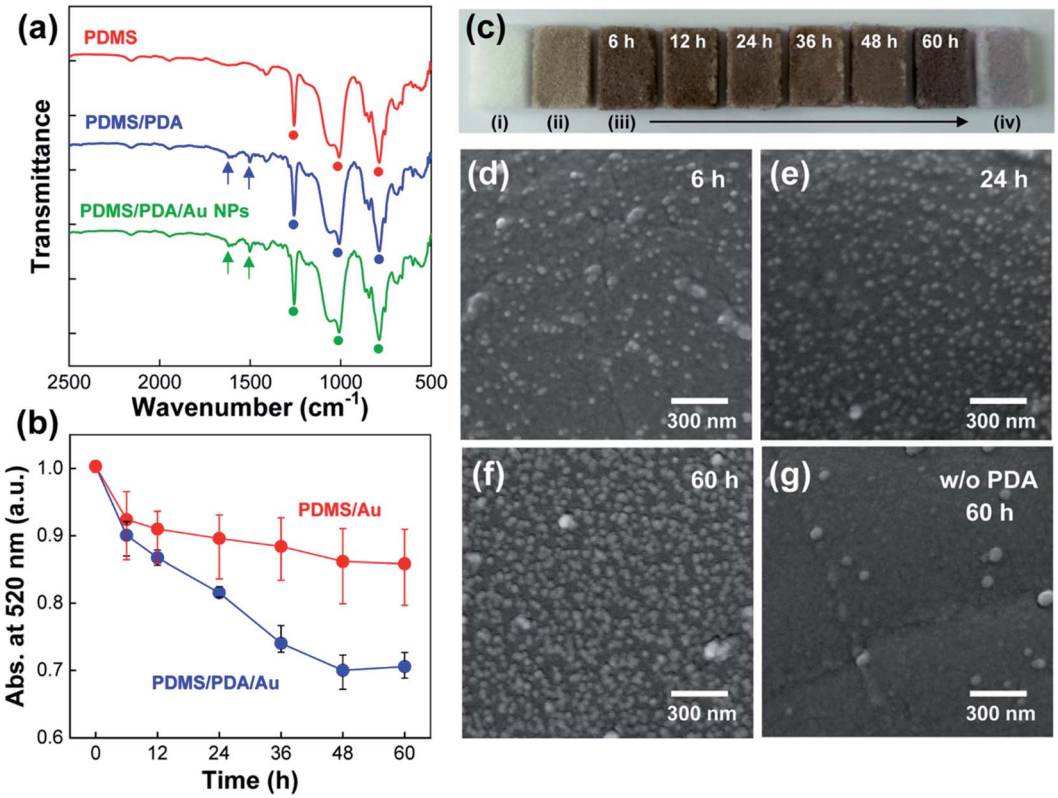

Fig. 2 (a) ATR-FTIR spectra of PDMS sponges with the introduction of PDA polymers and Au NPs. The PDMS/PDA was immersed in the NP solution for 24 h. (b) Time-dependent UV-Vis spectra after the immersion of PDMS (red color) and PDMS/PDA (blue color) in the NP solution. (c) Photographs of PDMS (i), PDMS/PDA (ii), PDMS/PDA/Au with different immersion times (iii), and PDMS/Au in the absence of PDA (iv). (d–f) Cross-sectional FE-SEM images of PDMS/PDA/Au sponges after immersion in NP solution for different times. (g) Cross-sectional FE-SEM images of PDMS/Au sponges after immersion in NP solution for 60 h.

reasonable to consider that dopamine monomers diffused inside the PDMS sponges for the homogenous PDA coating on the inner surface of the pores. To further confirm the synthesis of the PDA polymer, ATR-FTIR spectra were measured (Fig. 2a). For pristine PDMS sponges (red color), characteristic vibrational peaks corresponding to Si–CH_3, Si–O–Si, and Si–CH_3 groups were detected at 1260, 1011, and 790 cm^{-1}, respectively, (denoted as circles).[39] After the synthesis of PDA polymers on a PDMS sponge (blue color), the characteristic PDMS peaks were maintained (denoted as circles), and new vibrational peaks appeared at 1621 and 1508 cm^{-1} (denoted by arrows), which can be assigned to phenylic C=C stretching vibrations and N–H shearing vibrations of the PDA polymer.[40]

To introduce Au NPs into the PDMS sponges, PDA-coated PDMS sponges (denoted as PDMS/PDA for simplicity) were immersed in an aqueous solution of Au NPs for different periods of time (0–60 h). In this set of experiments, both PDMS sponges before and after PDA synthesis were immersed into the NP solution, and the absorbance peak of Au NPs at 520 nm was monitored at regular time intervals (Fig. 2b). It needs to be noted that the UV-Vis spectrum of Au NPs in H_2O was very stable and remained the same for an extended period of storage (more than one week). On the other hands, when PDMS/PDA or PDMS sponges were immersed in the NP solution, the absorbance peak of the NP solution was gradually reduced during the immersion. Since the adsorption of NPs onto the PDMS sponges reduces the concentration of Au NPs in a solution state, the decrease in peak intensity can be indicative of the amount of adsorbed NPs. In the case of PDA-coated PDMS, the absorbance value of colloidal Au NPs monotonically decreased and then saturated upon immersion (blue color in Fig. 2b). From the decrease of UV-Vis spectra, the concentration of Au NPs in PDMS/PDA/Au composites were evaluated as 0.013, 0.017, 0.023, 0.033, 0.038, 0.037 wt% with the immersion time of 6 h, 12 h, 24 h, 36 h, 48 h and 60 h, respectively. On the other hand, for pristine PDMS without PDA layer (red color), the absorption value was more or less maintained after the initial decrease. This comparison verified that PDA coating is necessary for the attachment of Au NPs onto the hydrophobic PDMS surface. The adsorption of Au NPs was further supported by the color

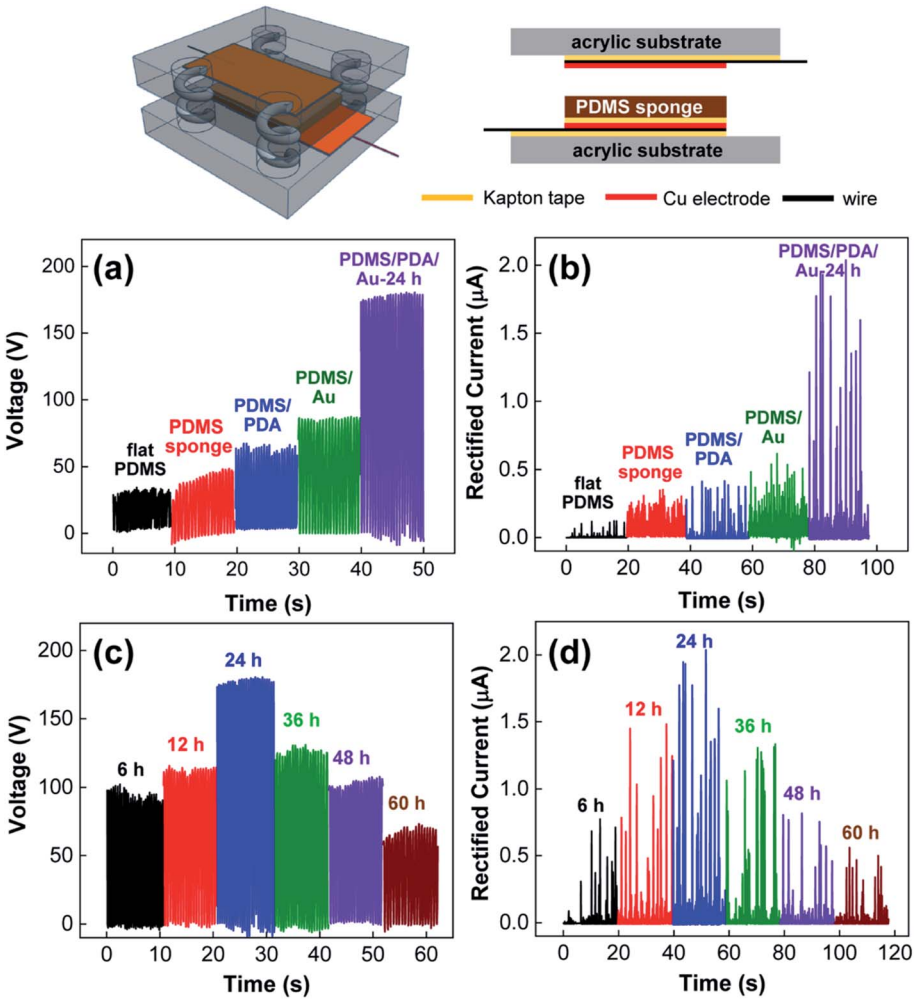

Fig. 3 (a) Open-circuit voltage and (b) short-circuit current of TENG devices prepared by flat PDMS (black), PDMS sponge (red), PDMS/PDA (blue), PDMS/Au (green), and PDMS/PDA/Au (purple) composites. (c) Open-circuit voltage and (d) short-circuit current of the TENG devices prepared by PDMS/PDA/Au composites under different immersion times. The structure of the TENG device is also included in the scheme.

changes of the PDMS sponges (Fig. 2c). As discussed, the color of the PDMS sponges changed from white ((i), in Fig. 2c) to pale brown (ii) after the PDA coating. Upon immersion in the NP solution, the color of PDMS became darker with the immersion time (iii) owing to the increased amount of Au NPs. In stark contrast, the color of PDMS was slightly changed to light purple in the absence of PDA coating due to the restricted adsorption of NPs onto the hydrophobic PDMS surface (iv). This slight color change can be ascribed to physically arrested NPs during water evaporation. The same result was also obtained by analyzing the cross-sectional FE-SEM images. In the presence of the PDA layer, the density of the adsorbed Au NPs on the PDMS surface noticeably increased with longer immersion time (Fig. 2d–f). However, the adsorption of NPs was strongly restricted on the hydrophobic PDMS surface without the adhesive PDA coating (Fig. 2g). Based on the results, PDA-coated PDMS sponges with the adsorbed Au NPs will be simply denoted as PDMS/PDA/Au NPs hereafter. We also noted that the PDMS/PDA/Au composites showed the same characteristic FTIR peaks of PDA and PDMS (green line in Fig. 2a).

After verifying the preparation of PDMS/PDA/Au sponges, we prepared TENG devices by assembling the composite PDMS sponges, Cu electrodes, and other components, as shown in the schematics of Fig. 3 (see details for the Experimental section). In the TENG structure, there was an air gap (~3 mm) between the top electrode and the air interface of the PDMS sponges to allow successive contact and separation under periodic compressive force. In addition, a flat PDMS film with the same thickness as the PDMS sponges (5 mm) was utilized for the TENG device for comparison. Fig. 3a shows the open-circuit voltage (V_{OC}) of the TENG with a series of composite PDMS sponges. As expected, the flat PDMS film without pores produced a very low output voltage with an average value of 33 V. With the successive introduction of pores, PDA coating, and Au NPs into the PDMS elastomers, the output performance of TENGs was systematically increased. In particular, PDMS/PDA/Au sponges (immersion time in NP solution = 24 h) produced V_{OC} with an average value of 180 V, which was enhanced by ~5.5-fold in comparison with flat PDMS. Also note, PDMS/Au sponges without PDA coatings enhanced the output voltage (65 V) in comparison with

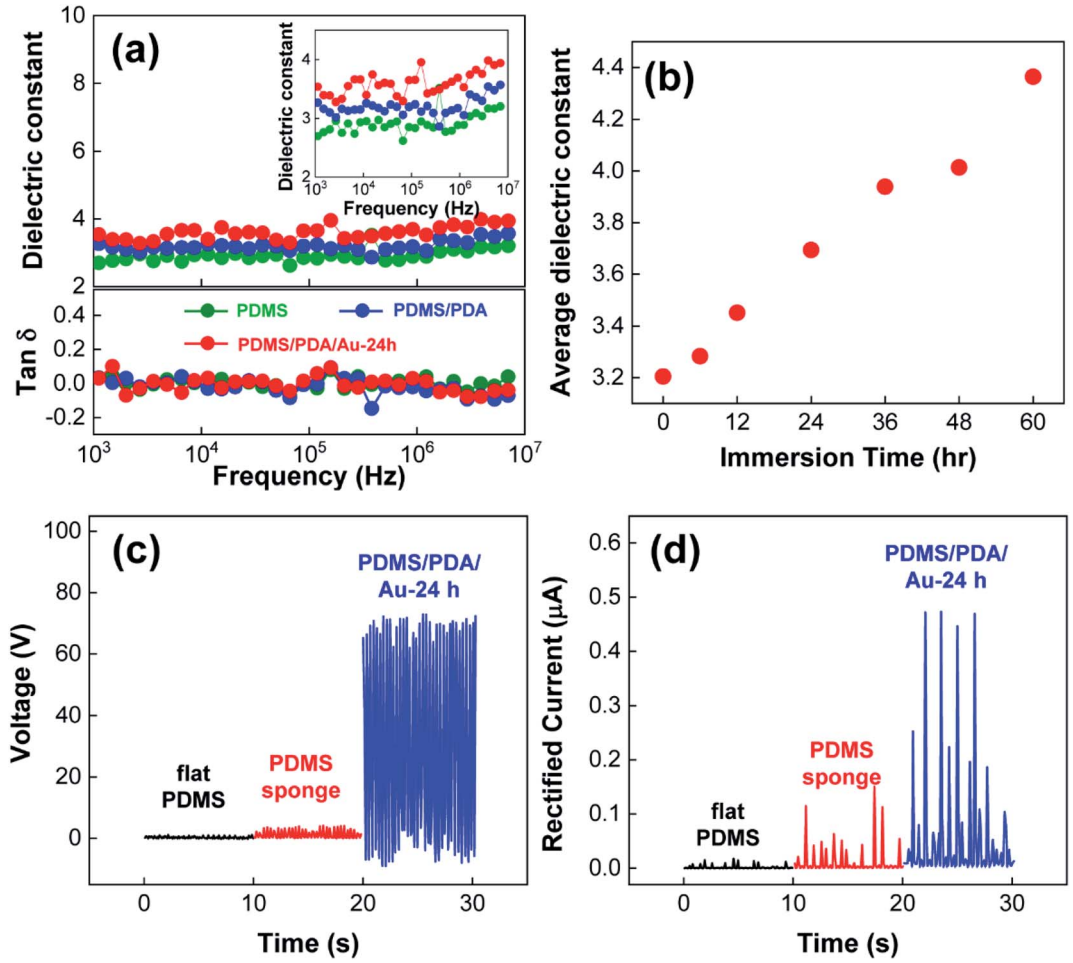

Fig. 4 (a) Frequency-dependent dielectric constant and loss tangent of PDMS sponge (green), PDMS/PDA (blue), and PDMS/PDA/Au (red) composites. (b) Average dielectric constant of PDMS/PDA/Au composites with different immersion times in aqueous solution of Au NPs. (c) Open-circuit voltage and (d) short-circuit current of gapless TENG devices based on flat PDMS (black), PDMS sponge (red), and PDMS/PDA/Au composites (blue) with immersion time = 24 h.

that of the pristine PDMS sponges (47 V), indicating the positive effect of the physically adsorbed Au NPs. A similar trend was observed in the short-circuit current (I_{SC}) measurement. In Fig. 3b, one can clearly observe the gradual current enhancement, which was accompanied by the introduction of pores, PDA coating, and Au NPs in the PDMS elastomers. Unfortunately, the precise measurement of I_{SC} was rather limited by (a) the sensitivity of our machine to detect the low current from TENGs and (b) non-identical local contacts inside the pores at each contact-separation step (this will be discussed later), which resulted in the non-uniform current response in Fig. 3b. Nevertheless, the gradual current enhancement from the corresponding TENG devices was identical to many independent preparations/measurements, confirming the enhanced TENG performance with pores and inorganic NPs.

To better understand the result, it should be noted that (a) the enhanced output performance is correlated with the charge density created on triboelectric materials during physical contact[3,4,8–15,17–25] and (b) TENG structures can be treated as an analogy of flat-panel capacitors.[17–19,22–25] This indicates that the created charge density (σ) is proportional to the capacitance of triboelectric materials (C).[17–19,21–25] Moreover, because the capacitance is proportional to the ratio of the dielectric constant (ε) to the thickness (d) of triboelectric materials as $C \sim \varepsilon/d$, experimental control on ε and d can increase the charge density as well as the TENG performance.[17–19,21–25] In our experiment, the introduction of pores can effectively reduce the thickness of PDMS sponges under external pressure. In addition, the introduction of Au NPs with a higher dielectric constant ($\varepsilon_{Au} = 6.0$) to PDMS ($\varepsilon_{PDMS} = 3.0$) can increase the dielectric constant of composite materials (ε).[17,18,22] To verify the enhancement in the dielectric constant, we measured the frequency-dependent dielectric permittivity of the PDMS composites over the frequency range of 10^3 to 10^7 Hz (Fig. 4a). For the porous PDMS sponges (green color), the average dielectric constant was 2.94. On the other hand, with the introduction of PDA layer (blue color) and Au NPs (red color, immersion time = 24 h), the dielectric constants of the composites PDMS sponges were gradually increased to 3.21 and 3.70, respectively. Meanwhile, the dielectric loss of the PDMS sponges were remained nearly unaltered after the addition of PDA layer and Au NPs (Fig. 4a), which indicated that the degree of conductance loss was not deteriorated. Therefore, it can be validated that ε/d has been collectively engineered to enhance the capacitance of composite PDMS sponges and the corresponding TENG performance without increasing dielectric loss.

To better study the influence of Au NPs, we utilized the composite PDMS/PDA/Au sponges prepared under different immersion conditions in the NP solution. As shown in Fig. 3c and d, both the output voltage and current initially increased and then decreased with the immersion time. According to the previous discussion, the introduction of more Au NPs into PDMS sponges allows for an increase in the dielectric constant, thereby enhancing the TENG performance. Indeed, the dielectric constant of the PDMS/PDA/Au sponges monotonically increased with immersion time (Fig. 4b). Also note, all the PDMS/PDA/Au composites in Fig. 3c and d have the same pore structures and thicknesses. Therefore, the decreased TENG performance under higher NP content could not be explained by the ε/d ratio value alone. Nevertheless, the trade-off trend can still be understood in terms of the created charge density. As discussed, the introduction of Au NPs can increase the charge density mainly by increasing the dielectric constant of the PDMS/PDA/Au composites. However, the presence of Au NPs on the surface of PDMS alternatively reduced the contact area between the top electrode and the air interface of the PDMS/PDA sponges. As shown in Fig. 2, the adsorbed Au NPs on the surface of the PDMS composites increased with the immersion time (further SEM images are shown in ESI Fig. S1†). Because the adsorbed Au NPs interfere with the effective triboelectric contact between PDMS and the Cu electrode, the high density of Au NPs on the surface would reduce the charge generation process. Consequently, Au NPs can be considered as either enhancers or reducers for TENG performance depending on the concentration.

The triboelectric charges were produced not only from the air surface but also inside the individual pores. To reveal the contribution of porous structures to the TENG performance, we prepared the same TENG devices as in the schematics of Fig. 3, but removed the air gap by directly attaching the air interface of the PDMS composite to the top electrode. Then, the periodic compressive force was applied to the gapless TENG devices to measure the output voltage and current (Fig. 4c and d). In the case of the flat PDMS film (black color), both V_{OC} and I_{SC} were quite negligible because the contact-separation process, which is mandatory for charge generation in triboelectric materials, was essentially inhibited. When a PDMS sponge is utilized (red color), a local contact-separation process can be allowed for each pore to produce additional charges on the pore surface. However, triboelectrification between homogenous material surfaces is inefficient, which results in a small enhancement in the electric output. In stark contrast, the PDMS/PDA/Au composite sponges produced strongly enhanced V_{OC} and I_{SC} (blue color), which clearly revealed the positive effect of Au NPs on the TENG performance. In the case of the PDMS/PDA/Au composites, the surface of each pore was decorated with Au NPs. Therefore, local contact between the Au NPs and PDA layer can be induced upon compression, which results in efficient charge transfer from Au NPs to the pore surface. As a result, the charge density in the pores could be strongly increased to improve the TENG performance. Nevertheless, it must be noted that the local contact inside the pores of PDMS/PDA/Au composites cannot be identical at each contact-separation cycle. Because the size and orientation of pores are irregular (see Fig. 1b), the vertical compression of the PDMS composites allows not only squeezing the pores but also sliding between pore surfaces. As a result, different types of contacts between (i) NPs and PDA, (ii) NPs and NPs, and (iii) PDA and PDA could be made at each contact-separation step. Since only the physical contact between NPs and PDA surfaces could efficiently contribute to the charge transfer, the generated charge density in the pores would be different at each contact-separation cycle. Therefore, the measured current would have different intensities in Fig. 3 and 4. In the similar way, the open-circuit voltage

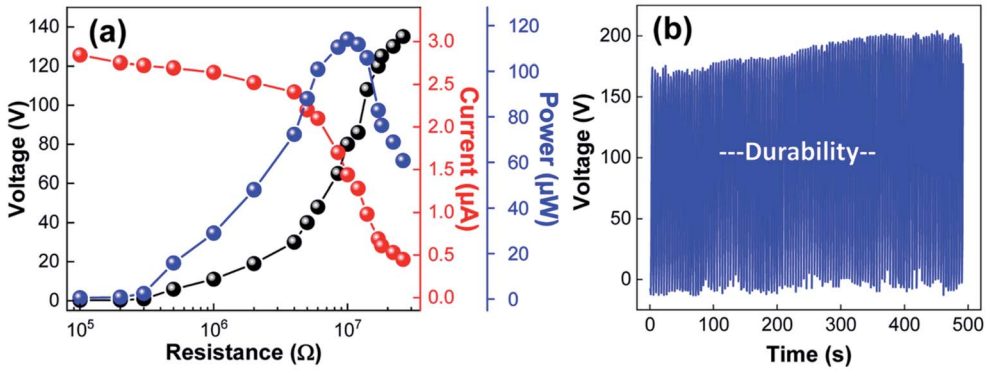

Fig. 5 (a) Output voltage (black), current (red), and power (blue) of the TENG with composite PDMS/PDA/Au sponge on the external load resistance. (b) Stability and durability test of the TENG under periodic contact-separation processes.

would be also affected by the different amount of charge generation in the pores, resulting in the non-uniform minimum value of V_{OC} in Fig. 4c.

Comparable results on gapless TENGs have been previously reported by the Baik group.[22] In their study, Au NPs were introduced to mesoporous PDMS sponges by evaporation. Since no specific chemical interaction has been utilized, Au NPs were placed at the bottom side of the pores by gravitational force. In this configuration, the local contact in the pores allowed charge transfer from Au NPs to PDMS, which produced negative charges on the top surface of the pores and negative charges on the Au NPs placed at the bottom side of the pores. As a result, the opposite charges were aligned with respect to each other, which brought about electrostatic induction to the electrodes for the TENG enhancement. However, in our study, Au NPs were homogeneously attached to the PDMS pores by the adhesive PDA layer, and the resulting positive/negative charges would be randomly distributed inside the pores. In this regard, it is more or less unclear how the pore charges could contribute to the electric output of TENG devices at the current stage.

To assess the prospects of the prepared TENGs, the voltage, current, and output power of TENGs with PDMS/PDA/Au composites (immersion time = 24 h) were measured under various external loads. As shown in Fig. 5a, the voltage increased with increasing external resistance, while the current decreased. As a result, the maximum power of the TENG reached a value of 115 μW at an external resistance of 10 MΩ. In addition, when the durability of the TENGs was examined under periodic contact-separation processes, the electric output was stable without noticeable degradation over 1500 cycles (Fig. 5b). This result strongly indicates the long-term stability of the composite PDMS/PDA/Au sponges. To better demonstrate the practical aspects, the TENGs with composite PDMS/PDA/Au sponges were connected to an array of commercial light-emitting diodes (LEDs) through a bridge rectifier. The power generated from the TENGs was able to turn on LEDs without charging capacitors. As shown in ESI Fig. S2,† the number of lighted LEDs initially increased but decreased with the immersion time, which additionally supported the discussed dual function of Au NPs in Fig. 3.

Conclusions

In this study, we demonstrated a simple and versatile method for enhancing TENG performance with composite PDMS sponges with Au NPs. Since the direct coating of Au NPs onto the PDMS surface was severely restricted by the chemical inertness of PDMS, PDA polymers have been introduced as an adhesive interface to promote homogenous adsorption of Au NPs on the inner surface of PDMS pores. Owing to the PDA layer, the amount of adsorbed NPs on the porous PDMS elastomers could be easily engineered by the immersion time, which resulted in a monotonic increase in the dielectric constant of the PDMS/PDA/Au composite sponges. The simultaneous control of both ε and d values with the composites PDMS/PDA/Au sponges substantially modified the TENG performance. When the amount of Au NPs was relatively small, the adsorbed NPs enhanced the electric output because of the increased dielectric constant as well as the additional charge generation inside the pores. However, further attachment of Au NPs to the PDMS surface deteriorated the TENG performance because they could interfere with contact charge generation in the triboelectric process. Because a variety of inorganic NPs could be adsorbed onto the PDA layer, further improvement in the TENG performance can be expected by introducing other high dielectric constant NPs to the porous PDMS structures, which would provide a better understanding of the triboelectricity and help the development of high-performance TENG devices.

Conflicts of interest

There are no conflicts of interest to declare.

Acknowledgements

This work has supported by the National Research Foundation of Korea (NRF) grant funded by the Korea government (MSIT) (NRF-2019R1A2C1086269). This work was supported by the Korea Institute of Energy Technology Evaluation and Planning (KETEP) and the Ministry of Trade, Industry & Energy (MOTIE) of the Republic of Korea (No. 20194010201840).

References

1 Y. Bai, H. Jantunen and J. Juuti, *Adv. Mater.*, 2018, **30**, 1707271.
2 M. Zhou, M. S. H. Al-Furjan, J. Zou and W. Liu, *Renewable Sustainable Energy Rev.*, 2018, **82**, 3582–3609.
3 C. Wu, A. C. Wang, W. Ding, H. Guo and Z. L. Wang, *Adv. Energy Mater.*, 2019, **9**, 1802906.
4 Z. L. Wang, *ACS Nano*, 2013, **7**, 9533–9557.
5 M. R. Sarker, S. Julai, M. F. M. Sabri, S. M. Said, M. M. Islam and M. Tahir, *Sens. Actuators, A*, 2019, **300**, 111634.
6 H. K. H. Lee, J. Wu, J. Barbé, S. M. Jain, S. Wood, E. M. Speller, Z. Li, F. A. Castro, J. R. Durrant and W. C. Tsoi, *J. Mater. Chem. A*, 2018, **6**, 5618–5626.
7 S. Yazdani and M. T. Pettes, *Nanotechnology*, 2018, **29**, 432001.
8 M.-L. Seol, S.-H. Lee, J.-W. Han, D. Kim, G.-H. Cho and Y.-K. Choi, *Nano Energy*, 2015, **17**, 63–71.
9 F.-R. Fan, L. Lin, G. Zhu, W. Wu, R. Zhang and Z. L. Wang, *Nano Lett.*, 2012, **12**, 3109–3114.
10 J.-H. Zhang, Y. Li, J. Du, X. Hao and H. Huang, *J. Mater. Chem. A*, 2019, **7**, 11724–11733.
11 P. Zhao, N. Soin, K. Prashanthi, J. Chen, S. Dong, E. Zhou, Z. Zhu, A. A. Narasimulu, C. D. Montemagno, L. Yu and J. Luo, *ACS Appl. Mater. Interfaces*, 2018, **10**, 5880–5891.
12 Z.-H. Lin, G. Zhu, Y. S. Zhou, Y. Yang, P. Bai, J. Chen and Z. L. Wang, *Angew. Chem., Int. Ed.*, 2013, **52**, 5065–5069.
13 X. Li, Z.-H. Lin, G. Cheng, X. Wen, Y. Liu, S. Niu and Z. L. Wang, *ACS Nano*, 2014, **8**, 10674–10681.
14 G. Song, Y. Kim, S. Yu, M.-O. Kim, S.-H. Park, S. M. Cho, D. B. Velusamy, S. H. Cho, K. L. Kim, J. Kim, E. Kim and C. Park, *Chem. Mater.*, 2015, **27**, 4749–4755.
15 S.-H. Shin, Y. H. Kwon, Y.-H. Kim, J.-Y. Jung, M. H. Lee and J. Nah, *ACS Nano*, 2015, **9**, 4621–4627.
16 L. S. McCarty and G. M. Whitesides, *Angew. Chem., Int. Ed.*, 2008, **47**, 2188–2207.
17 J. Chen, H. Guo, X. He, G. Liu, Y. Xi, H. Shi and C. Hu, *ACS Appl. Mater. Interfaces*, 2016, **8**, 736–744.
18 X. He, H. Guo, X. Yue, J. Gao, Y. Xi and C. Hu, *Nanoscale*, 2015, **7**, 1896–1903.
19 J. W. Lee, H. J. Cho, J. Chun, K. N. Kim, S. Kim, C. W. Ahn, I. W. Kim, J.-Y. Kim, S.-W. Kim, C. Yang and J. M. Baik, *Sci. Adv.*, 2017, **3**, e1602902.
20 D. Kim, S.-J. Park, S.-B. Jeon, M.-L. Seol and Y.-K. Choi, *Adv. Electron. Mater.*, 2016, **2**, 1500331.
21 K. Y. Lee, J. Chun, J.-H. Lee, K. N. Kim, N.-R. Kang, J.-Y. Kim, M. H. Kim, K.-S. Shin, M. K. Gupta, J. M. Baik and S.-W. Kim, *Adv. Mater.*, 2014, **26**, 5037–5042.
22 J. Chun, J. W. Kim, W.-S. Jung, C.-Y. Kang, S.-W. Kim, Z. L. Wang and J. M. Baik, *Energy Environ. Sci.*, 2015, **8**, 3006–3012.
23 X. Xia, J. Chen, H. Guo, G. Liu, D. Wei, Y. Xi, X. Wang and C. Hu, *Nano Res.*, 2017, **10**, 320–330.
24 X. He, X. Mu, Q. Wen, Z. Wen, J. Yang, C. Hu and H. Shi, *Nano Res.*, 2016, **9**, 3714–3724.
25 K. Shi, H. Zou, B. Sun, P. Jiang, J. He and X. Huang, *Adv. Funct. Mater.*, 2020, **30**, 1904536.
26 M. Pusty, A. Sharma, L. Sinha, A. Chaudhary and P. Shirage, *ChemistrySelect*, 2017, **2**, 2774–2782.
27 M. Pusty, L. Sinha and P. M. Shirage, *New J. Chem.*, 2019, **43**, 284–294.
28 M. Pusty and P. M. Shirage, *RSC Adv.*, 2020, **10**, 10097–10112.
29 G. Lu, H. Li and H. Zhang, *Chem. Commun.*, 2011, **47**, 8560–8562.
30 U. Cataldi, R. Caputo, Y. Kurylyak, G. Klein, M. Chekini, C. Umeton and T. Bürgi, *J. Mater. Chem. C*, 2014, **2**, 7927–7933.
31 J. H. Ryu, P. B. Messersmith and H. Lee, *ACS Appl. Mater. Interfaces*, 2018, **10**, 7523–7540.
32 H. Lee, S. M. Dellatore, W. M. Miller and P. B. Messersmith, *Science*, 2007, **318**, 426–430.
33 H. Luo, C. Gu, W. Zheng, F. Dai, X. Wang and Z. Zheng, *RSC Adv.*, 2015, **5**, 13470–13477.
34 S.-J. Choi, T.-H. Kwon, H. Im, D.-I. Moon, D. J. Baek, M.-L. Seol, J. P. Duarte and Y.-K. Choi, *ACS Appl. Mater. Interfaces*, 2011, **3**, 4552–4556.
35 M. Zakia, H. Song, C. H. Song, S.-M. Jin, E. Lee, Y. S. Won, K. Kim, K.-S. Kim, J. Yoon and S. I. Yoo, *J. Mater. Chem. C*, 2019, **7**, 5051–5058.
36 P. K. Jain, X. Huang, I. H. El-Sayed and M. A. El-Sayed, *Plasmonics*, 2007, **2**, 107–118.
37 X. Liu, M. Atwater, J. Wang and Q. Huo, *Colloids Surf., B*, 2007, **58**, 3–7.
38 P. Xue, Q. Li, Y. Li, L. Sun, L. Zhang, Z. Xu and Y. Kang, *ACS Appl. Mater. Interfaces*, 2017, **9**, 33632–33644.
39 D. Sharma, W. Jia, F. Long, S. Pati, Q. Chen, Y. Qyang, B. Lee, C. K. Choi and F. Zhao, *Bioact. Mater.*, 2019, **4**, 142–150.
40 J. Hu, S. Wu, Q. Cao and W. Zhang, *RSC Adv.*, 2016, **6**, 81767–81773.